A&A 604, A93 (2017)
DOI: 10.1051/0004-6361/201629687

Astronomy & Astrophysics

Constraining galaxy cluster velocity field with the thermal Sunyaev-Zel'dovich and kinematic Sunyaev-Zel'dovich cross-bispectrum

G. Hurier[1,2]

[1] Centro de Estudios de Física del Cosmos de Aragón (CEFCA), Plaza de San Juan, 1, planta 2, 44001 Teruel, Spain
e-mail: ghurier@cefca.es
[2] Institut d'Astrophysique Spatiale, CNRS (UMR 8617) Université Paris-Sud 11, Bâtiment 121, 91405 Orsay, France

Received 11 September 2016 / Accepted 11 March 2017

ABSTRACT

The Sunyaev-Zel'dovich (SZ) effects are produced by the interaction of cosmic microwave background (CMB) photons with the ionized and diffuse gas of electrons inside galaxy clusters integrated along the line of sight. The two main effects are the thermal SZ (tSZ) produced by thermal pressure inside galaxy clusters and the kinematic SZ (kSZ) produced by peculiar motion of galaxy clusters compared to CMB rest-frame. The kSZ effect is particularly challenging to measure as it follows the same spectral behavior as the CMB, and consequently cannot be separated from the CMB using spectral considerations. In this paper, we explore the feasibility of detecting the kSZ through the computation of the tSZ-CMB-CMB cross-correlation bispectrum for current and future CMB experiments. We conclude that the next generation of CMB experiments will offer the possibility to detect the tSZ-kSZ-kSZ bispectrum at high signal-to-noise ration (S/N). This measurement will constraints the intra-cluster dynamics and the velocity field of galaxy cluster that is extremely sensitive to the growth rate of structures and thus to dark energy properties. Additionally, we also demonstrate that the tSZ-kSZ-kSZ bispectrum can be used to break the degeneracies between the mass-observable relation and the cosmological parameters to set tight constraints, up to 4%, on the $Y - M$ relation calibration.

Key words. large-scale structure of Universe – cosmic background radiation – cosmological parameters – galaxies: clusters: intracluster medium – galaxies: clusters: general

1. Introduction

Present cosmic microwave background (CMB) experiments such as ACTT (Sievers et al. 2013), SPT (Bleem et al. 2015), and *Planck* (Planck Collaboration I 2016) have mapped the CMB primary temperature anisotropies with unprecedented precision, and constrained cosmological parameters from the CMB angular power-spectrum analyses (see e.g., Sievers et al. 2013; Planck Collaboration XIII 2016; de Haan et al. 2016). However, the measurement of secondary anisotropies, such as the Sunyaev-Zel'dovich (SZ) effects (Sunyaev & Zeldovich 1972), is still limited by the noise level and angular resolution in current experiments.

Thanks to it's spectral behavior, the tSZ effect can be isolated from the CMB and foreground emissions (Remazeilles et al. 2011; Hurier et al. 2013). The thermal SZ (tSZ) effect, produced by thermal electron in intra-cluster medium, has been shown as a powerful probe to detect galaxy clusters (Hasselfield et al. 2013; Bleem et al. 2015; Planck Collaboration XXVII 2016), and to constrain cosmological parameters using large-scale structure matter distribution (Hasselfield et al. 2013; Mantz et al. 2015; Planck Collaboration XXIV 2016; Planck Collaboration XXII 2016; de Haan et al. 2016). However, cosmological constraints obtained via the tSZ effect strongly depend on the mass-observable relation. Assuming a value of $b = 0.2$ (Planck Collaboration XXIV 2016) for the hydrostatic mass bias, the observed number of galaxy clusters on the sky is only half of the predicted number assuming CMB-derived cosmological parameters (Planck Collaboration XIII 2016). CMB-derived cosmological parameter, favours a hydrostatic mass bias of $b = 0.3$–0.5. Thus, methodology to break the degeneracy between cosmological parameters and the mass-observable relation needs to be investigated further to test the consistency of the ΛCDM cosmological model.

After the tSZ effect, the second dominant source of arcminute-scale anisotropies is the kinematic SZ (kSZ) effect (Ostriker & Vishniac 1986), produced by the peculiar motion of galaxy clusters with respect to CMB rest-frame. The kSZ is approximately ten times fainter than the tSZ effect and contrary to the tSZ effect, it cannot be separated from the CMB signal using spectral considerations. Consequently, the measurement of this kSZ effect is significantly harder than the one of the tSZ effect. The kSZ effect is directly related to the peculiar velocity field of the matter distribution and the baryonic matter density. Thus, this effect presents significantly different cosmological dependancies than the tSZ effect, especially with the universe growth rate (Sugiyama et al. 2017), which is a powerful probe to understand the CMB-LSS tension for cosmological parameter estimation.

Several approaches have been proposed to recover the kSZ effect: (i) Direct measurement of anisotropies in the CMB angular power spectrum at high-ℓ (see Addison et al. 2013; George et al. 2015, for recent results); (ii) the pairwise momentum estimator, using the preferential motion of one large-scale structure toward another large-scale structure (Peebles 1980; Diaferio et al. 2000); (iii) inverting the continuity equation

relating density and velocity fields (Ho et al. 2009; Kitaura et al. 2012); and (iv) cross-correlation bispectrum between CMB and cosmic shear (Doré et al. 2004) or galaxy surveys (DeDeo et al. 2005)

Evidence of the kSZ effect angular power spectrum has been found using the CMB angular power spectrum (George et al. 2015) and combining the tSZ angular power-spectrum and bispectrum (Crawford et al. 2014). The kSZ detection has been achieved in two cases: for individual galaxy cluster internal dynamics (Sayers et al. 2013; Adam et al. 2017), and for a statistical sample of galaxy clusters using pairwise momentum (Hand et al. 2012; Hernández-Monteagudo et al. 2015; Soergel et al. 2016). Recent studies (see e.g., Hernández-Monteagudo et al. 2015) achieve statistical detection at approximately 5σ significance level.

The kSZ effect produces a non-Gaussian contribution to the CMB anisotropies. High-order statistics have been shown as a powerful probe to detect the tSZ effect (see e.g., Wilson et al. 2012; Hill & Sherwin 2013; Planck Collaboration XXII 2016). In this paper, we explore the possibility to detect the tSZ-kSZ-kSZ cross-correlation bispectrum for the next generation of CMB experiments. First, in Sect. 2 we present tSZ and kSZ effects, and in Sect. 3 we detail the computation of tSZ and kSZ power spectra. Then, in Sect. 4 we present the modeling of the tSZ and kSZ bispectra. Finally, in Sect. 5 we present our forecasts for next generation CMB experiments.

2. The SZ effects

The tSZ effect is a distortion of the CMB black body radiation through inverse Compton scattering. CMB photons receive an average energy boost by collision with hot (a few keV) ionized electrons of the intra-cluster medium (see e.g., Birkinshaw 1999; Carlstrom et al. 2002, for reviews). The thermal SZ Compton parameter in a given direction, $\boldsymbol{n}$, on the sky is given by

$$y(\boldsymbol{n}) = \int n_\mathrm{e} \frac{k_\mathrm{B} T_\mathrm{e}}{m_\mathrm{e} c^2} \sigma_\mathrm{T} \, \mathrm{d}s, \tag{1}$$

where k_B is the Boltzmann constant, c the speed of light, m_e the electron mass, σ_T the Thomson cross-section, $\mathrm{d}s$ the distance along the line-of-sight, $\boldsymbol{n}$, and n_e and T_e are the electron number density and temperature, respectively. In units of CMB temperature the contribution of the tSZ effect for a given observation frequency ν is

$$\frac{\Delta T_\mathrm{CMB}}{T_\mathrm{CMB}} = g(\nu)\, y, \tag{2}$$

where T_CMB is the CMB temperature, and $g(\nu)$ the tSZ spectral dependance. Neglecting relativistic corrections we have

$$g(\nu) = \left[x \coth\left(\frac{x}{2}\right) - 4 \right], \tag{3}$$

with $x = h\nu/(k_\mathrm{B} T_\mathrm{CMB})$. At $z = 0$, where $T_\mathrm{CMB}(z=0) = 2.726 \pm 0.001$ K (Mather et al. 1999), the tSZ effect is negative below 217 GHz and positive for higher frequencies.

The kSZ effect produces a shift of the CMB black body radiation temperature but causes whiteout of spectral distortion. Contrary to tSZ effect, it thus possesses the same spectral energy distribution (SED) as the CMB primordial anisotropies and cannot be separated from them. The kinetic SZ-induced temperature anisotropies in a given direction on the sky is given by

$$k(\boldsymbol{n}) = \int n_\mathrm{e} \frac{\boldsymbol{v} \cdot \boldsymbol{n}}{c} \sigma_\mathrm{T} \, \mathrm{d}s, \tag{4}$$

with $\boldsymbol{v}$ the peculiar velocity vector of the galaxy cluster. The total kSZ flux from a cluster is proportional to the gas mass, $M_\mathrm{gas,500}$ of the cluster, and modulated by the scalar product $\boldsymbol{v} \cdot \boldsymbol{n}$ that ranges from $-v$ to v.

3. Power spectra

3.1. General formalism

The angular cross power spectrum between two maps reads

$$C_\ell^{XY} = \frac{1}{2\ell+1} \sum_m \frac{1}{2} \left(x_{\ell m} y^*_{\ell m} + x^*_{\ell m} y_{\ell m} \right), \tag{5}$$

with $x_{\ell m}$ and $y_{\ell m}$, the coefficients from the spherical harmonics decomposition of the two maps concerned, and ℓ the multipole of the spherical harmonic expansion. In the context of large-scale structure tracers, we model this cross-correlation, as well as the auto correlation power spectra, assuming the following general expression

$$C_\ell^{XY} = C_\ell^{XY-1\mathrm{h}} + C_\ell^{XY-2\mathrm{h}}, \tag{6}$$

where $C_\ell^{XY-1\mathrm{h}}$ is the Poissonian contribution and $C_\ell^{XY-2\mathrm{h}}$ is the two-halo term. These terms can be computed considering a mass function formalism. The mass function, $\mathrm{d}^2N/\mathrm{d}M\mathrm{d}V$, gives the number of dark matter halos (in this paper we consider the fitting formula from Tinker et al. 2008) as a function of the halo mass and redshift.

The Poissonian term can be computed by assuming the Fourier transform of normalized halo projected profiles of X and Y, weighted by the mass function and the respective fluxes of the halo for X and Y observables (see e.g., Cole & Kaiser 1988; Komatsu & Seljak 2002, for a derivation of the tSZ auto-correlation angular power spectrum).

$$C_\ell^{XY-1\mathrm{h}} = 4\pi \int \mathrm{d}z \frac{\mathrm{d}V}{\mathrm{d}z\mathrm{d}\Omega} \int \mathrm{d}M \frac{\mathrm{d}^2N}{\mathrm{d}M\mathrm{d}V} X_{500} Y_{500} x_\ell y_\ell, \tag{7}$$

where X_{500} and Y_{500} are the average fluxes of the halo in X and Y maps that depend on the critical mass of the galaxy cluster, M_{500}, the redshift, z, and can be obtained with scaling relations, and $\mathrm{d}V/\mathrm{d}z\mathrm{d}\Omega$, the comoving volume element. The Fourier transform of a 3D profile projected across the line-of-sight on the sphere reads, $\frac{4\pi r_\mathrm{s}}{l_\mathrm{s}^2} \int_0^\infty \mathrm{d}x\, x^2 p(x) \frac{\sin(\ell x/\ell_\mathrm{s})}{\ell x/\ell_\mathrm{s}}$, where $p(x)$ is the halo 3D profile in X or Y maps, $x = r/r_\mathrm{s}$, $\ell_\mathrm{s} = D_\mathrm{ang}(z)/r_\mathrm{s}$, and r_s is the scale radius of the profile.

The two-halo term corresponds to large-scale fluctuations of the dark matter field, that induce correlations in the halo distribution over the sky. It can be computed as (see e.g., Komatsu & Kitayama 1999; Diego & Majumdar 2004; Taburet et al. 2011)

$$C_\ell^{XY-2\mathrm{h}} = 4\pi \int \mathrm{d}z \frac{\mathrm{d}V}{\mathrm{d}z\mathrm{d}\Omega} \left(\int \mathrm{d}M \frac{\mathrm{d}^2N}{\mathrm{d}M\mathrm{d}V} X_{500} x_\ell b(M_{500}, z) \right) \times \left(\int \mathrm{d}M \frac{\mathrm{d}^2N}{\mathrm{d}M\mathrm{d}V} Y_{500} y_\ell b(M_{500}, z) \right) P_{X,Y}(k, z), \tag{8}$$

with $b(M_{500}, z)$, the time dependent linear bias that relates the power spectrum between X and Y distribution, $P_{X,Y}(k, z)$, to the underlying dark matter power spectrum. Following Mo & White (1996), Komatsu & Kitayama (1999) we adopt

$$b(M_{500}, z) = 1 + (\nu^2(M_{500}, z) - 1)/\delta_\mathrm{c}(z),$$

with $\nu(M_{500}, z) = \delta_\mathrm{c}(z) / \left[D_\mathrm{g}(z) \sigma(M_{500}) \right]$, $D_\mathrm{g}(z)$, the linear growth factor, and $\delta_\mathrm{c}(z)$, the over-density threshold for spherical collapse.

Table 1. Scaling-law parameters and error budget for both $Y_{500} - M_{500}$ (Planck Collaboration XXIX 2014) and $Y_{500} - T_{500}$ (Planck Collaboration XXIX 2014) relations.

$M_{500} - Y_{500}$		$M_{500} - T_{500}$	
$\log Y_\star$	–0.19 ± 0.02	$\log T_\star$	–4.27 ± 0.02
α_{sz}	1.79 ± 0.08	α_T	2.85 ± 0.18
β_{sz}	0.66 ± 0.50	β_T	1
$\sigma_{\log Y}$	0.075 ± 0.010	$\sigma_{\log T}$	0.14 ± 0.02

3.2. The tSZ and kSZ scaling relations

A key step in the modeling of the cross-correlation between tSZ and kSZ is to relate the mass, M_{500}, and the redshift, z, of a given cluster to tSZ flux, Y_{500}, and kSZ flux, K_{500}. The cross-correlation between tSZ and kSZ effects is thus highly dependent on the $M_{500} - Y_{500}$ and the $M_{500} - K_{500}$ relations in terms of normalization and slope. Consequently, we need to use the relations derived from a representative sample of galaxy clusters, with careful propagation of statistical and systematic uncertainties. However, such observational constraints are not available for the kSZ effect. We stress that for power spectrum analysis, the intrinsic scatter of such scaling laws has to be considered, because it will produce extra power that has to be accounted for in order to avoid biases.

We used the $M_{500} - Y_{500}$ scaling laws presented in Planck Collaboration XXIX (2014):

$$E^{-\beta_{sz}}(z)\left[\frac{D_A^2(z)Y_{500}}{10^{-4}\,\mathrm{Mpc}^2}\right] = Y_\star\left[\frac{h}{0.7}\right]^{-2+\alpha_{sz}}\left[\frac{(1-b)M_{500}}{6\times10^{14}\,M_\odot}\right]^{\alpha_{sz}}, \quad (9)$$

with h the dimensionless Hubble parameter, D_A the angular distance, and $E(z) = \Omega_m(1+z)^3 + \Omega_\Lambda$. The coefficients $Y_\star$, α_{sz}, and β_{sz} from Planck Collaboration XXIX (2014), are given in Table 1. We used $b = 0.2$ for the bias between X-ray-estimated mass and effective mass of the clusters.

We also need to have an estimate of the cluster temperature, T_{500}. In this work, we used the scaling law from Planck Collaboration XI (2011):

$$E(z)^{-\beta_T}Y_{500} = T_\star\left[\frac{T_{500}}{6\,\mathrm{keV}}\right]^{\alpha_T}, \quad (10)$$

where the coefficients $T_\star$, α_T , and β_T are given in Table 1.

To model the $K_{500} - M_{500}$ relation, we consider the relation from DeDeo et al. (2005) for the velocity field:

$$v_k = i\frac{H(z)D_g}{1+z}\frac{\mathrm{dln}(D_g)}{\mathrm{dln}(a)}\frac{\delta_k}{k}, \quad (11)$$

and consequently for the velocity dispersion

$$\sigma_v(M_{500},z) = \frac{H(z)D_g}{1+z}\frac{\mathrm{dln}(D_g)}{\mathrm{dln}(a)}\sigma_{-1}, \quad (12)$$

with D_g the growth factor and $\sigma_j(z)$ is defined for any integer j as

$$\sigma_j(M_{500}) = \frac{1}{2\pi^2}\int \mathrm{d}k\, k^{2(1+j)}P(k)W^2(kR), \quad (13)$$

where $W(kR) = \frac{3}{(kR)^3}(\sin(kR) - kR\cos(kR))$ is the Fourier transform of the real space top-hat window function, with $R = \sqrt{\frac{3M_{500}}{4\pi\bar{\rho}}}$, where $\bar{\rho}$ is the critical density of the universe.

By simplicity, to estimate the kSZ flux root-mean-square (over velocities), K_{500}, we consider the relation

$$Y_{500} \simeq K_{500}\frac{k_B T_{500}}{m_e c^2}\left(\frac{\sigma_v}{c}\right)^{-1}. \quad (14)$$

K_{500} is proportional to $M_{gas,500}$, thus the $K_{500} - M_{500}$ and $M_{gas,500} - M_{500}$ intrinsic scatters are identical. The extra scatter induced by the velocities is accounted by the σ_v factor. We derived a $K_{500}-M_{500}$ intrinsic scatter of $\sigma_{\log K} = 0.03\pm0.01$ from the galaxy cluster sample presented in Planck Collaboration XI (2011).

Additionally, the $Y_{500}-M_{500}$ and $K_{500}-M_{500}$ intrinsic scatters are correlated. The intrinsic scatters follow the relation

$$\sigma^2_{\log YK} = \sigma^2_{\log Y} + \sigma^2_{\log K} - 2\rho\sigma_{\log Y}\sigma_{\log K}, \quad (15)$$

where $\sigma_{\log YK} = 0.08 \pm 0.01$ is the intrinsic scatter of the $Y_{500} - K_{500}$ (equivalent to the scatter of the $Y_{500} - M_{gas,500}$) and ρ is the correlation factor between $Y_{500} - M_{500}$ and $K_{500} - M_{500}$ intrinsic scatters. For consistency, we used $\sigma_{\log Y} = 0.10 \pm 0.01$ that has been derived on the galaxy cluster sample from Planck Collaboration XI (2011). We derived $\rho \in [0.5, 1.0]$. In the following we assume $\rho = 0.75$.

3.3. Log-normal scatter and n-point correlation functions

Scaling relations shown in Sect. 3.2 presents an intrinsic physical scatter (see Table 1). This scatter is generally considered as a log-normal distribution. When entering in correlation functions, this log-normal scatter will act as an additional source of power. This additional power, for a quantity X, can be expressed as a relation between $\langle X^n\rangle$ and $X_\star$, where $X_\star$ is the log-normal mean of the X variable. In the most general case, the nth momentum, $M^{(n)}$, expectation of a set of N variable X_i can be written

$$M^{(n)} = \left\langle\prod_i^N X_i^{n_i}\right\rangle$$
$$\left\langle M^{(n)}\right\rangle = A_{\mathrm{norm}}\int\prod_i^N X_i^{n_i}\mathrm{d}X_i \times\exp\left(-\frac{[\log(\boldsymbol{X})-\log(\boldsymbol{X}_\star)]^{\mathrm{T}}C_S^{-1}[\log(\boldsymbol{X})-\log(\boldsymbol{X}_\star)]}{2}\right), \quad (16)$$

where A_{norm} is the normalization factor of the log-normal distribution, C_S is the scaling relation scatter covariance matrix, $\boldsymbol{X}$ is a vector of X_i variables, $\boldsymbol{X}_\star$ is a vector containing the log-normal expectation $X_{\star,i}$ for each variable X_i, and n_i is the order of each variable X_i in the momentum $M^{(n)}$ and satisfies $\sum_i^N n_i = n$. It can be easily shown that

$$\left\langle M^{(n)}\right\rangle = \exp\left(\frac{\boldsymbol{n}^{\mathrm{T}}C_S\boldsymbol{n}}{2}\right)\prod_i^N X_{\star,i}^{n_i}, \quad (17)$$

where $\boldsymbol{n}$ is a vector of n_i. This effect produces a power enhancement of 6% for the tSZ bispectrum, which is significant for high-signal-to-noise ration (S/N) measurements of tSZ bispectrum. For the tSZ-kSZ-kSZ bispectrum, we derived a power enhancement of 1.8%. In the following, we correct all spectra for this effect.

Table 2. Amplitude of the different terms' contribution to the tSZ and kSZ power spectra and bispectra.

	1-halo	2-halo	3-halo
$C_\ell^{\mathrm{tSZ-kSZ}}$	0	0	
$C_\ell^{\mathrm{kSZ-kSZ}}$	1/3	P_B	
$b^{\mathrm{tSZ-tSZ-kSZ}}_{\ell_1\ell_2\ell_3}$	0	(0, 0, 0)	0
$b^{\mathrm{tSZ-kSZ-kSZ}}_{\ell_1\ell_2\ell_3}$	1/3	(P_B, P_B, P_m/3)	B_k
$b^{\mathrm{kSZ-kSZ-kSZ}}_{\ell_1\ell_2\ell_3}$	0	(0, 0, 0)	0

Notes. P_B is the power spectrum of the momentum field and P_m the matter power spectrum.

3.4. Pressure and density profiles

The tSZ effect is directly proportional to the pressure integrated across the line of sight. In this work, we model the galaxy cluster pressure profile by a generalized Navarro Frenk and White (GNFW, Navarro et al. 1997; Nagai et al. 2007) profile of the form

$$\mathbb{P}(r) = \frac{P_0}{(c_{500}r)^\gamma\,[1 + (c_{500}r)^\alpha]^{(\beta-\gamma)/\alpha}}. \tag{18}$$

For the parameters c_{500}, α, β, and γ, we used the best-fitting values from Arnaud et al. (2010) presented in Table 1. The absolute normalization of the profile P_0 is set assuming the scaling laws $Y_{500} - M_{500}$ presented in Sect. 3.2.

To model the kSZ profile, we need the density, $n_\mathrm{e}(r)$, profile. Thus, we assume a polytropic equation of state (see, e.g., Komatsu & Seljak 2001), $\mathbb{P}(r) = n_\mathrm{e}(r)T_\mathrm{e}(r)$, with $n_\mathrm{e}(r) \propto T_\mathrm{e}(r)^\delta$ where δ is the polytropic index. Considering that the kSZ varies with n_e, the kSZ profile is proportional to $P(r)^{\epsilon_p}$, where $\epsilon_p = \frac{\delta}{\delta+1}$ ranges from 0.5 to 1.0 for $1.0 < \delta < \infty$.

The overall normalization of kSZ profile is deduced from the scaling law $K_{500} - M_{500}$ presented in Sect. 3.2.

3.5. tSZ and kSZ power spectra

The kSZ effect is dependent on the orientation of the peculiar velocity vector. Consequently, power spectra have to be averaged over orientations. In Table 2, we present the multiplicative factors to be applied on kSZ-related power spectra, where P_B is the power spectrum of the momentum field and P_m is the power spectrum of the matter field. We notice that kSZ effects present a two-halo term, induced by the large-scale correlations between the velocities of different clusters.

In Fig. 1, we present the power density as a function of M_{500} and z for the tSZ and kSZ power spectra, the tSZ bispectrum, and the tSZ-kSZ-kSZ cross-bispectrum. We observe that the tSZ power spectrum samples higher mass and lower redshift than the kSZ power spectrum; this effect is a consequence of the slope of $Y_{500} - M_{500}$ (1.7) and $K_{500} - M_{500}$ (1). We also observe that bispectra give more weight to very massive and nearby objects.

4. Bispectra

Combining tSZ and kSZ, it is possible to build two auto-correlation bispectra, and two cross-correlation bispectra. In this work we aim at predicting the tSZ-kSZ-kSZ bispectrum, thus our modeling only accounts for non-Gaussian objects that correlate with the tSZ effect. Consequently, we only consider the kSZ effect from virialized halos and we neglect the kSZ contribution produced by diffuse baryons at higher redshift.

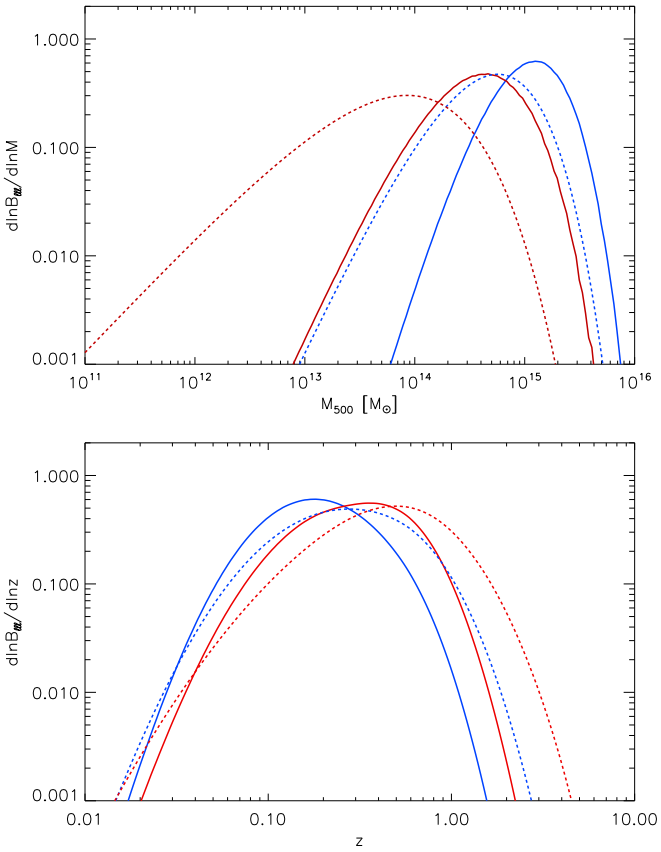

Fig. 1. Power density as a function of M_{500} (*top panel*) and redshift (*bottom panel*) for the tSZ power spectrum (dotted blue line), the tSZ bispectrum (solid blue line), the kSZ power spectrum (dotted red line), and the tSZ-kSZ-kSZ bispectrum (solid red line).

4.1. Cross-correlation bispectra

Following the same halo model approach, we can easily predict the SZ bispectra (see Bhattacharya et al. 2012, for a detailed description of the tSZ bispectrum). In halo model formalism, a bispectrum can be separated into three terms: one-halo, two-halo, and three-halo, as

$$b^{XYZ}_{\ell_1\ell_2\ell_3} = b^{XYZ-1\mathrm{h}}_{\ell_1\ell_2\ell_3} + b^{XYZ-2\mathrm{h}}_{\ell_1\ell_2\ell_3} + b^{XYZ-3\mathrm{h}}_{\ell_1\ell_2\ell_3}. \tag{19}$$

The one-halo term, is produce by the auto-correlation of a cluster with itself,

$$b^{XYZ-1\mathrm{h}}_{\ell_1\ell_2\ell_3} = 4\pi \int \mathrm{d}z \frac{\mathrm{d}V}{\mathrm{d}z\mathrm{d}\Omega} \int \mathrm{d}M \frac{\mathrm{d}^2N}{\mathrm{d}M\mathrm{d}V} X_{500}Y_{500}Z_{500}x_{\ell_1}y_{\ell_2}z_{\ell_3}. \tag{20}$$

The two-halo involves two points from the same halo and a third from another one. As a consequence, this term receives three

contributions,

$$
\begin{aligned}
b^{XYZ-2h}_{\ell_1\ell_2\ell_3} = 4\pi &\int \mathrm{d}z \frac{\mathrm{d}V}{\mathrm{d}z\mathrm{d}\Omega} P_{XY,Z}(k,z) \\
&\times \left(\int \mathrm{d}M \frac{\mathrm{d}^2N}{\mathrm{d}M\mathrm{d}V} X_{500} Y_{500} x_{\ell_1} y_{\ell_2} b(M_{500},z) \right) \\
&\times \left(\int \mathrm{d}M \frac{\mathrm{d}^2N}{\mathrm{d}M\mathrm{d}V} Z_{500} z_{\ell_3} b(M_{500},z) \right) \\
&+ 4\pi \int \mathrm{d}z \frac{\mathrm{d}V}{\mathrm{d}z\mathrm{d}\Omega} P_{XZ,Y}(k,z) \\
&\times \left(\int \mathrm{d}M \frac{\mathrm{d}^2N}{\mathrm{d}M\mathrm{d}V} X_{500} Z_{500} x_{\ell_1} z_{\ell_3} b(M_{500},z) \right) \\
&\times \left(\int \mathrm{d}M \frac{\mathrm{d}^2N}{\mathrm{d}M\mathrm{d}V} Y_{500} y_{\ell_2} b(M_{500},z) \right) \\
&+ 4\pi \int \mathrm{d}z \frac{\mathrm{d}V}{\mathrm{d}z\mathrm{d}\Omega} P_{YZ,X}(k,z) \\
&\times \left(\int \mathrm{d}M \frac{\mathrm{d}^2N}{\mathrm{d}M\mathrm{d}V} Y_{500} Z_{500} y_{\ell_2} z_{\ell_3} b(M_{500},z) \right) \\
&\times \left(\int \mathrm{d}M \frac{\mathrm{d}^2N}{\mathrm{d}M\mathrm{d}V} X_{500} x_{\ell_1} b(M_{500},z) \right). \qquad (21)
\end{aligned}
$$

The three-halo involves the correlation of three different halos,

$$
\begin{aligned}
b^{XYZ-3h}_{\ell_1\ell_2\ell_3} = 4\pi &\int \mathrm{d}z \frac{\mathrm{d}V}{\mathrm{d}z\mathrm{d}\Omega} B_{X,Y,Z}(k_1,k_2,k_3,z) \\
&\times \left(\int \mathrm{d}M \frac{\mathrm{d}^2N}{\mathrm{d}M\mathrm{d}V} X_{500} x_{\ell_1} b_3(M_{500},z) \right) \\
&\times \left(\int \mathrm{d}M \frac{\mathrm{d}^2N}{\mathrm{d}M\mathrm{d}V} Y_{500} y_{\ell_2} b_3(M_{500},z) \right) \\
&\times \left(\int \mathrm{d}M \frac{\mathrm{d}^2N}{\mathrm{d}M\mathrm{d}V} Z_{500} z_{\ell_3} b_3(M_{500},z) \right) \qquad (22)
\end{aligned}
$$

with $B_{X,Y,Z}(k_1,k_2,k_3,z)$ being the bispectrum of X, Y, and Z distribution, and $b_3(M_{500},z)$ being the bias that relates dark-matter and halo distributions.

4.2. The tSZ and kSZ cross-bispectrum

The tSZ-tSZ-kSZ bispectrum has a null expectation due to the average over all the directions for the momentum field of galaxy clusters. Table 2 lists the relative amplitude of each contribution.

For the prediction of the tSZ-kSZ-kSZ two-halo term, we compute the momentum field power spectrum similarly to Shaw et al. (2012). The tSZ-kSZ-kSZ bispectrum two-halo term involves three contributions; two of which where the two considered halos receive contribution from the kSZ effect. These terms involve the momentum field power spectrum. The third contribution involves the correlation between a halo weighted by its tSZ flux and a halo weighed by the square of the kSZ effect. Consequently, this third contribution involves the matter power spectrum that describes the distribution of halos over the sky, weighted by the average over momentum directions (similarly to the kSZ power spectrum). For the 3-halo term matter-momentum bispectrum we used the prescription from (DeDeo et al. 2005).

We studied the cosmological parameter dependancies of this cross bispectrum. We found that the tSZ-kSZ-kSZ bispectrum is proportional to $\Omega_\mathrm{m}^{4.1}\sigma_8^{10.1}H_0^{2.0}$. By comparison the tSZ bispectrum is proportional to $\Omega_\mathrm{m}^{3.9}\sigma_8^{12.9}H_0^{-1.1}$ and $\ell \simeq 1000$. Then, tSZ-kSZ-kSZ might be a powerful probe to break degeneracies between cosmological parameters and scaling relations by providing similar cosmological dependencies to the tSZ power spectrum with significantly different astrophysical process dependencies. We also note that the tSZ bispectrum presents similar degeneracies to the tSZ power spectrum. Consequently, it cannot be used to break degeneracies between cosmology and astrophysical processes.

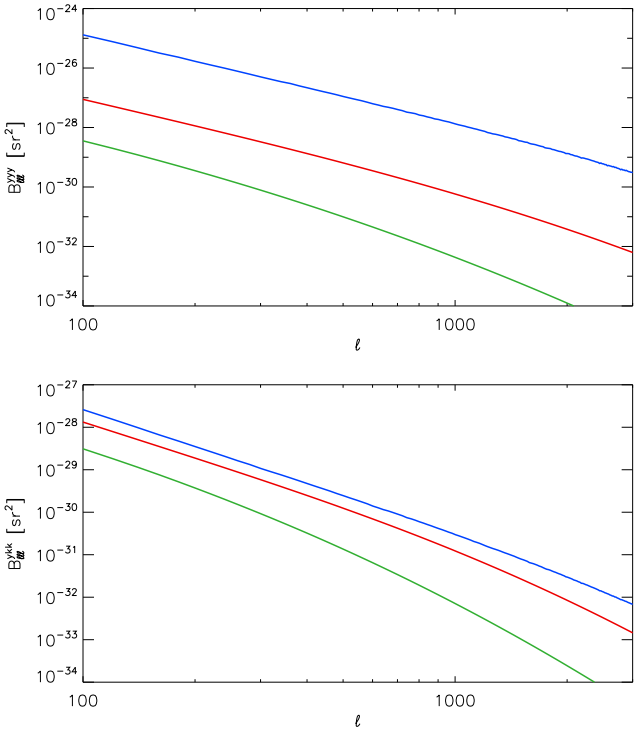

Fig. 2. tSZ (*top panel*) and tSZ-kSZ-kSZ (*bottom panel*) bispectra 1-halo term (blue line), 2-halo term (red line), and 3-halo term (green line).

In Fig. 1, we present the power density for tSZ and tSZ-kSZ-kSZ bispectra. We observe that bispectra are sensitive to higher mass and lower redshift than power spectra. We note that the tSZ-kSZ-kSZ bispectrum and tSZ power spectrum present similar power density distribution as a function of mass and redshift. The tSZ-kSZ-kSZ bispectrum is thus sensitive to galaxy clusters with mass ranging from 10^{14} and 10^{15} $M_\odot$, at $z < 1$.

We present the tSZ and tSZ-kSZ-kSZ bispectra in Fig. 2. We observed that for the tSZ bispectrum, the one-halo term is two orders of magnitude higher than the two-halo term. Consequently, for the tSZ bispectrum, two-halo and three-halo terms can be safely neglected. This is consistent with the tSZ angular power spectrum that only presents significant contribution from the two-halo term at very low-ℓ. When using higher-order statistics we favor higher mass, lower-z objects that are less frequent over the sky. Indeed, the one-halo term amplitude evolved with the number, N_cl, that significantly contributes to the spectra, where the two-halo term evolves as N_cl^2 and the three-halo term as N_cl^3.

Contrary to the tSZ bispectrum, the tSZ-kSZ-kSZ bispectrum two-halo and three-halo terms present significant contributions compared to the one-halo term. This higher contribution is explained by the fact that the kSZ effect favors lower-mass and higher-z objects than the tSZ effect, as shown in Fig. 1.

4.3. Uncertainties and optimal estimator

To compute the bispectrum between three maps X, Y, and Z, we considered the following formula

$$b_{\ell_1\ell_2\ell_3} = \frac{1}{f_{\rm sky}} \sum_{\boldsymbol{n}} X_{\ell_1} Y_{\ell_2} Z_{\ell_3}, \tag{23}$$

where X_{ℓ_1}, Y_{ℓ_2}, and Z_{ℓ_3} are the real space map that only contain ℓ_1, ℓ_2, ℓ_3 multipoles of maps X, Y, Z respectively, $f_{\rm sky}$ is the covered sky fraction, and $\boldsymbol{n}$ is the direction over the sky.

This estimator is known to reduce the variance of the bispectrum without biasing the expectation of the bispectrum. We note that, in the case of a cross-correlation bispectrum ℓ_1, ℓ_2, ℓ_3 are not commutative quantities.

Then the bispectrum variance in the weak non-Gaussian limit can be expressed as

$$\begin{aligned}\left\langle b_{\ell_1\ell_2\ell_3}, b_{\ell'_1\ell'_2\ell'_3}\right\rangle = &\frac{C^{XX}_{\ell_1} C^{YY}_{\ell_2} C^{ZZ}_{\ell_3}}{f_{\rm sky} N_{\ell_1,\ell_2,\ell_3}} \delta_{\ell_1\ell'_1}\delta_{\ell_2\ell'_2}\delta_{\ell_3\ell'_3} \\ &+ \frac{C^{XX}_{\ell_1} C^{YZ}_{\ell_2} C^{ZY}_{\ell_3}}{f_{\rm sky} N_{\ell_1\ell_2\ell_3}} \delta_{\ell_1\ell'_1}\delta_{\ell_2\ell'_3}\delta_{\ell_3\ell'_2} \\ &+ \frac{C^{XY}_{\ell_1} C^{YX}_{\ell_2} C^{ZZ}_{\ell_3}}{f_{\rm sky} N_{\ell_1\ell_2\ell_3}} \delta_{\ell_1\ell'_2}\delta_{\ell_2\ell'_1}\delta_{\ell_3\ell'_3} \\ &+ \frac{C^{XY}_{\ell_1} C^{YZ}_{\ell_2} C^{ZX}_{\ell_3}}{f_{\rm sky} N_{\ell_1\ell_2\ell_3}} \delta_{\ell_1\ell'_2}\delta_{\ell_2\ell'_3}\delta_{\ell_3\ell'_1} \\ &+ \frac{C^{XZ}_{\ell_1} C^{YY}_{\ell_2} C^{ZX}_{\ell_3}}{f_{\rm sky} N_{\ell_1\ell_2\ell_3}} \delta_{\ell_1\ell'_3}\delta_{\ell_2\ell'_2}\delta_{\ell_3\ell'_1} \\ &+ \frac{C^{XZ}_{\ell_1} C^{YX}_{\ell_2} C^{ZY}_{\ell_3}}{f_{\rm sky} N_{\ell_1\ell_2\ell_3}} \delta_{\ell_1\ell'_3}\delta_{\ell_2\ell'_1}\delta_{\ell_3\ell'_2}, \end{aligned} \tag{24}$$

with $N_{\ell_1\ell_2\ell_3}$, being the number of modes for the (ℓ_1, ℓ_2, ℓ_3) triangle.

For our purpose, we considered the tSZ-kSZ-kSZ bispectrum, thus we have two points that are identical. Considering that the expectation of tSZ and kSZ cross-correlation power spectrum, $C_\ell^{\rm tSZ,kSZ}$, is zero, we can safely neglect this term in the computation of uncertainties. In this context Eq. (24) reduces to

$$\begin{aligned}\left\langle b_{\ell_1\ell_2\ell_3}, b_{\ell'_1\ell'_2\ell'_3}\right\rangle = &\frac{C^{XX}_{\ell_1} C^{XX}_{\ell_2} C^{ZZ}_{\ell_3}}{f_{\rm sky} N_{\ell_1,\ell_2,\ell_3}} \delta_{\ell_1\ell'_1}\delta_{\ell_2\ell'_2}\delta_{\ell_3\ell'_3} \\ &+ \frac{C^{XX}_{\ell_1} C^{XX}_{\ell_2} C^{ZZ}_{\ell_3}}{f_{\rm sky} N_{\ell_1\ell_2\ell_3}} \delta_{\ell_1\ell'_2}\delta_{\ell_2\ell'_1}\delta_{\ell_3\ell'_3}. \end{aligned} \tag{25}$$

If we have $\ell_1 = \ell_2$ then

$$\langle b_{\ell_1\ell_2\ell_3}, b_{\ell_1\ell_2\ell_3}\rangle = 2\frac{C^{XX}_{\ell_1} C^{XX}_{\ell_2} C^{ZZ}_{\ell_3}}{f_{\rm sky} N_{\ell_1\ell_2\ell_3}}, \tag{26}$$

and if we have $\ell_1 \neq \ell_2$ then

$$\langle b_{\ell_1\ell_2\ell_3}, b_{\ell_1\ell_2\ell_3}\rangle = \frac{C^{XX}_{\ell_1} C^{XX}_{\ell_2} C^{ZZ}_{\ell_3}}{f_{\rm sky} N_{\ell_1\ell_2\ell_3}}. \tag{27}$$

4.4. Foreground contamination

The two main foreground contaminations in SZ analyses are the CIB and extra-galactic radio sources.

CIB leakage in tSZ and CMB maps is composed of high-z CIB sources. As a consequence, CIB in such maps is almost Gaussian and will not significantly bias the results. The level of CIB in the final bispectrum can be estimated through the different shape of CIB and SZ bispectra Lacasa (2014).

Radio sources with a significant flux are in small number on the microwave sky. It has been shown in tSZ bispectra analyses (Planck Collaboration XXI 2014) that the results are not biased by radio sources that would produce a negative bias due to the way radio sources leak in tSZ maps (Hurier et al. 2013).

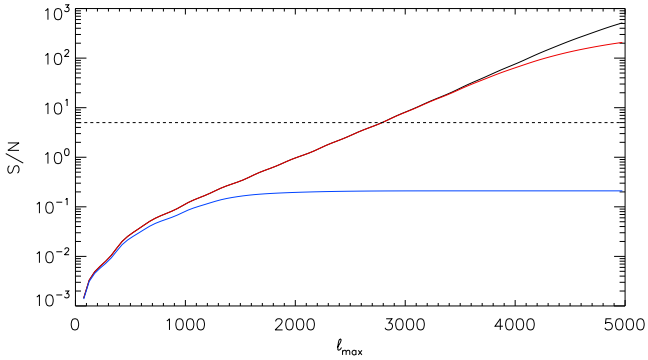

Fig. 3. Cumulative S/N for the tSZ-kSZ-kSZ bispectrum as a function of ℓ for a cosmic-variance-limited experiment (black line), the Planck experiment (blue line), and a COrE+ like experiment (red line). The dashed line shows the 5σ level.

5. Forecasts

5.1. Cosmic-variance-limited experiment

In a first step, we estimated the expected signal-to-noise ratio considering a sky composed by tSZ, kSZ, and CMB anisotropies. Indeed tSZ can be extracted from other components (Hurier et al. 2013), but the kSZ signal cannot be distinguished from the CMB primary anisotropies or secondary anisotropies that follow the CMB black body emission law. We also consider $f_{\rm sky} = 0.5$. This choice of a small sky fraction is used to avoid foreground residual contamination that contaminates tSZ and CMB signals.

We present in Fig. 3 the expected cumulative S/N as a function of the multipole ℓ. We observed that the tSZ-kSZ-kSZ can be detected for scales above $\ell \simeq 3000$.

5.2. Realistic CMB experiments

The Planck experiments have produced a cosmic-variance limited measurement of the CMB temperature angular power spectrum (Planck Collaboration XV 2014). However, secondary anisotropies (such as the tSZ effect) measurements are still dominated by instrumental noise. In this section we present the expected S/N from the Planck experiment and from a future COrE+[1] like CMB mission.

5.2.1. *Planck*-like experiment

To estimate the expected S/N using data from a *Planck*-like mission, we used the noise level from *Planck* public CMB (Planck Collaboration IX 2016) and tSZ (Planck Collaboration XXII 2016) maps assuming $f_{\rm sky} = 0.5$. For both CMB and tSZ maps we used the total measured power-spectra to estimate the

[1] http://hdl.handle.net/11299/169642

noise level in the tSZ-kSZ-kSZ bispectrum. Consequently, this estimation of the noise level accounts for CIB and point source contamination in both tSZ and CMB maps.

In Fig. 3, we present the expected signal-to-noise as a function of the maximum ℓ considered. We observe that Planck is expected to achieve a 0.2σ measurement of the tSZ-kSZ-kSZ bispectrum. This rules out the possibility of extracting this signal from the Planck data. The main limitations are the noise level in tSZ and CMB maps, residual from other astrophysical components (mainly the CIB for the tSZ map), and the angular resolution of Planck maps, 5 arcmin FWHM for the CMB maps and 10 arcmin for the tSZ maps. The CMB also strongly limits the sensitivity at low-ℓ. In Fig. 3, we can see low-ℓ oscillations that correspond to the CMB acoustic oscillation pics contributing to the noise for the tSZ-kSZ-kSZ bispectrum.

5.2.2. Future CMB experiments

We now consider a future CMB spacecraft mission assuming specificities (frequencies, noise level per detector, number of detectors, beams) for a COrE+ like experiment, and a sky coverage $f_{\rm sky} = 0.5$. For such a future experiment, we do not have direct access to CMB or tSZ map noise levels. Thus, we computed the expected noise level in component-separated maps obtained through linear combination of multi-frequency intensity maps. The optimal noise level, V_i, for a single astrophysical component is given by,

$$V_i = \left(\boldsymbol{F}_i C_N^{-1} \boldsymbol{F}_i^T \right)^{-1}, \tag{28}$$

where $\boldsymbol{F}_i$ is the component spectral behavior in the frequency channels of the experiment, and C_N^{-1} is the instrumental noise covariance matrix. We assume that C_N^{-1} is diagonal, and that multiple detectors at a given frequency have uncorrelated noise.

However, there are several components on the sky. Thus, we use the following equation

$$\mathcal{V} = \left(\mathcal{F} C_N^{-1} \mathcal{F}^T \right)^{-1}, \tag{29}$$

where $\mathcal{F}$ is a rectangular matrix containing the astrophysical component spectral behavior. In this analysis, we considered:

- the tSZ effect;
- the CMB;
- one thermal dust component, that follows a modified blackbody SED (SED) with a temperature, $T_{\rm d} = 20$ K, and spectral index $\beta_{\rm d} = 1.6$;
- one radio component following a ν^{α_r} SED with a spectral index $\alpha_{\rm r} = -1$;
- the CO component;
- the spinning dust component.

Additionally, some components, such as the cosmic-infrared-background (CIB), cannot be modeled with a single spectral law and contribute as a partially correlated component from frequency to frequency. We thus model the CIB contribution to the final variance as

$$\mathcal{V} = \left(\mathcal{F} \left[C_N + C_{\rm CIB} \right]^{-1} \mathcal{F}^T \right)^{-1}, \tag{30}$$

where $C_{\rm CIB}$ is the CIB covariance matrix. We computed the CIB covariance matrix using the model presented in (Planck Collaboration XXIII 2016). For a more realistic estimation we performed the noise estimation as a function of the multipole ℓ to have an estimate of the noise power-spectrum in CMB and tSZ maps. We verified that this approach is realistic by applying it to the *Planck* mission specificities and comparing to the noise level observed in *Planck* tSZ and CMB public maps.

In Fig. 3, we present the expected tSZ-kSZ-kSZ bispectrum S/N for a COrE+ like experiment. We observe that the tSZ-kSZ-kSZ S/N is dominated by the cosmic variance up to $\ell = 4000$. We can expect a detection up to 200σ when neglecting potential systematic effects in the CMB and tSZ maps. We also stress that our estimation of the tSZ-kSZ-kSZ bispectrum may underestimate the real signal at high-ℓ, where the internal dynamics of the gas inside galaxy clusters will most likely add extra power on small scales.

In Fig. 4, we present the expected constraints on $\Omega_{\rm m}$, σ_8, and $Y_\star$ when combining the measurement of tSZ power spectrum, bispectrum, and tSZ-kSZ-kSZ bispectrum.

The Likelihood function is computed as follows,

$$\mathcal{L} \propto \exp\left(- \left[\boldsymbol{D} - \boldsymbol{M}(\sigma_8, \Omega_{\rm m}, Y_\star) \right]^{\rm T} C_{\rm SZ} \left[\boldsymbol{D} - \boldsymbol{M}(\sigma_8, \Omega_{\rm m}, Y_\star) \right] \right), \tag{31}$$

where $\boldsymbol{D}$ is a vector containing the tSZ-tSZ-tSZ and tSZ-kSZ-kSZ bispectra for our fiducial model ($\sigma_8 = 0.8$, $\Omega_{\rm m} = 0.3$, $\Delta Y_\star / Y_\star = 0$), $\boldsymbol{M}$ is a vector containing the two bispectra for parameters (σ_8, $\Omega_{\rm m}$, $\Delta Y_\star / Y_\star$), and $C_{\rm SZ}$ is the covariance matrix of the two bispectra in the weakly non-Gaussian limit (see Eq. (24)). The correlation between the tSZ-tSZ-tSZ and tSZ-kSZ-kSZ bispectra in the weakly non-Gaussian limit is proportional to $\left(C_\ell^{\rm tSZ,kSZ} \right)^2$, thus contraints from the tSZ-tSZ-SZ bispectrum and from the tSZ-kSZ-kSZ bispectrum can be considered as independent. Figure 4 shows the expected constraints when σ_8, $\Omega_{\rm m}$, and $Y_\star$ are allowed to vary. We marginalized over $H_0 = 67.8 \pm 0.9$ km s^{-1} Mpc^{-1} and fixed all other parameters.

We observed that σ_8 and $\Omega_{\rm m}$ present a high degree of degeneracy, as our three probes present similar degeneracies for these two parameters. However, we observed that we can achieve a precision of 4% on $Y_\star$ without any external prior. Such an approach will allow us to calibrate the tSZ scaling relation without the need for X-ray hydrostatic mass.

6. Conclusion and discussion

We have proposed a new method to detect kSZ effect using future high-resolution CMB experiments. This method presents the advantage of being sensitive to the galaxy cluster velocity dispersion without bias from CMB auto-correlation or from kSZ effect produced by the diffuse baryonic gas at high redshift. This method also allows to constrain the velocity field without a selection function. By comparison, the kSZ angular power spectrum measured by George et al. (2015), is sensitive to the total kSZ power spectrum. The constraints achieved on the kSZ power spectrum by Crawford et al. (2014) when combining tSZ power spectrum and bispectrum is an indirect constraint, and is affected by a strong cosmic variance, as it measures the tSZ-tSZ-tSZ and tSZ-kSZ-kSZ bispectra as a single quantity.

The method proposed in the present paper, relies on direct measurement of the tSZ-kSZ-kSZ bispectrum after a separation of the tSZ and kSZ signals. Consequently, it allows us to obtain a model-independent and low-cosmic-variance estimation of the tSZ-kSZ-kSZ bispectrum.

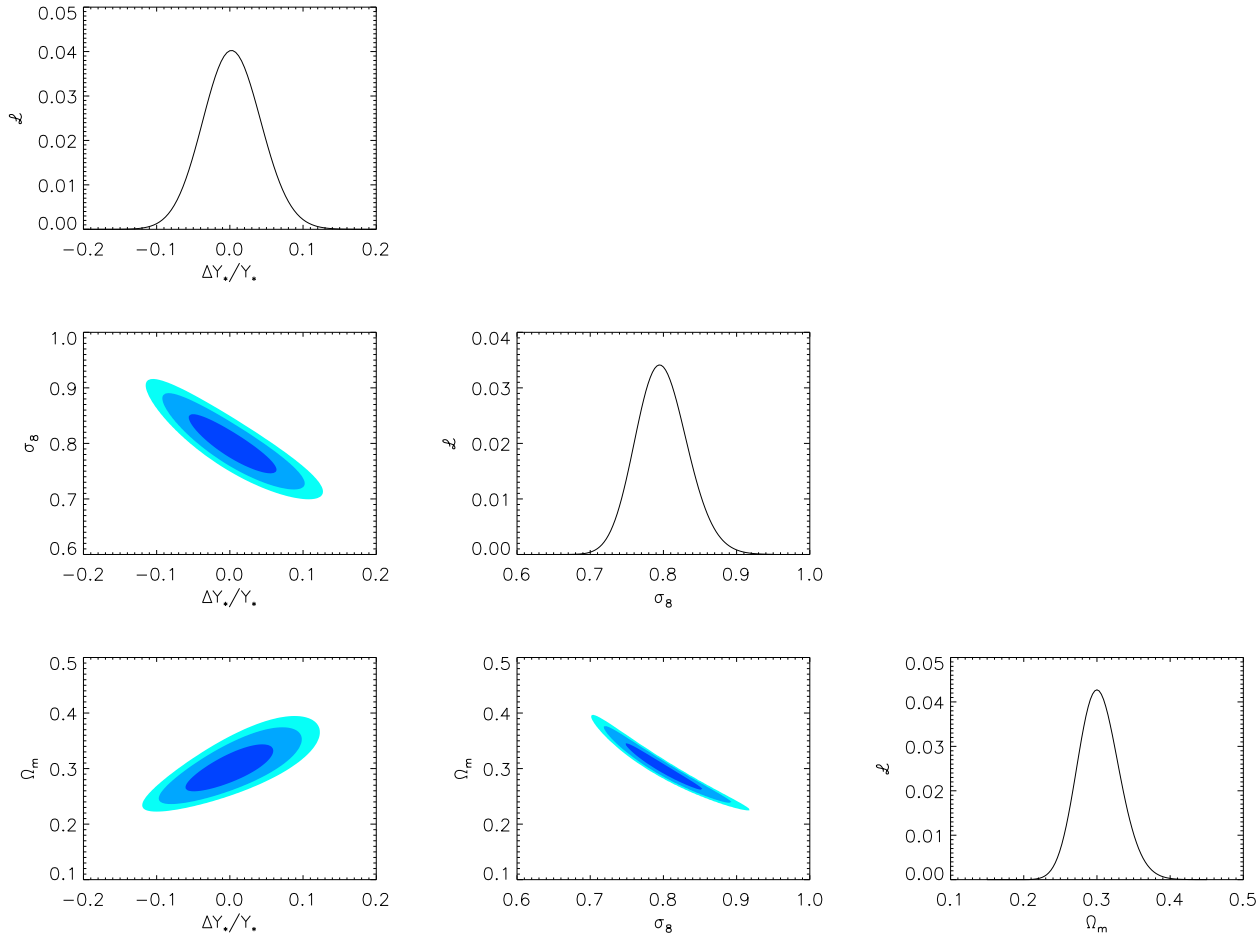

Fig. 4. Likelihood for combined tSZ power spectrum, bispectrum, and tSZ-kSZ-kSZ bispectrum as a function of $Y_\star$, σ_8, and Ω_m. Dark blue, blue, and light blue contours indicate the 1, 2, and 3σ levels.

We have presented a complete modeling of the tSZ-kSZ-kSZ bispectrum and deduced the associated cosmological parameter dependencies. We derived the dependencies of the tSZ-kSZ-kSZ and tSZ bispectra with respect to cosmological parameters. Previous works have also discussed the tSZ bispectrum scaling with cosmological parameters (see e.g., Bhattacharya et al. 2012; Crawford et al. 2014) and found slightly different scaling. The cosmological dependencies of the tSZ angular power spectrum are highly dependent on the weighting given to each halo. As a consequence, differences on the mass-observable relation will significantly affect the bispectrum scaling with respect to cosmological parameters. This also explains the scale dependance of the bispectrum scalings. Indeed, different angular scales receive contribution from halos at differeérent redshifts and masses.

We also demonstrated that future experiments, will be sensitive to the tSZ-kSZ-kSZ cross-correlation bispectrum up to 200σ.

We demonstrated that the tSZ-kSZ-kSZ bispectrum can be combined with the tSZ power spectrum and bispectrum to set tight constraints (4%) on the $Y - M$ relation calibration and thus on the hydrostatic mass bias. This will enable the possibility of setting cosmological constraints without the need for prior on the hydrostatic mass bias, which is a crucial step considering that the hydrostatic mass-bias is the main limitation for cosmological parameter estimation from tSZ surveys.

Acknowledgements. The author thanks F.Lacasa for useful discussions. We acknowledge the support of the French "Agence Nationale de la Recherche" under grant ANR-11-BD56-015.

References

Adam, R., Bartalucci, I., Pratt, G. W., et al. 2017, A&A, 598, A115
Addison, G. E., Dunkley, J., & Bond, J. R. 2013, MNRAS, 436, 1896
Arnaud, M., Pratt, G. W., Piffaretti, R., et al. 2010, A&A, 517, A92
Bhattacharya, S., Nagai, D., Shaw, L., Crawford, T., & Holder, G. P. 2012, ApJ, 760, 5
Birkinshaw, M. 1999, Phys. Rep., 310, 97
Bleem, L. E., Stalder, B., de Haan, T., et al. 2015, ApJS, 216, 27
Carlstrom, J. E., Holder, G. P., & Reese, E. D. 2002, ARA&A, 40, 643
Cole, S., & Kaiser, N. 1988, MNRAS, 233, 637
Crawford, T. M., Schaffer, K. K., Bhattacharya, S., et al. 2014, ApJ, 784, 143
de Haan, T., Benson, B. A., Bleem, L. E., et al. 2016, ApJ, 832, 95
DeDeo, S., Spergel, D. N., & Trac, H. 2005, ArXiv e-prints [arXiv:astro-ph/0511060]
Diaferio, A., Sunyaev, R. A., & Nusser, A. 2000, ApJ, 533, L71
Diego, J. M., & Majumdar, S. 2004, MNRAS, 352, 993
Doré, O., Hennawi, J. F., & Spergel, D. N. 2004, ApJ, 606, 46
George, E. M., Reichardt, C. L., Aird, K. A., et al. 2015, ApJ, 799, 177
Hand, N., Addison, G. E., Aubourg, E., et al. 2012, Phys. Rev. Lett., 109, 041101
Hasselfield, M., Hilton, M., Marriage, T. A., et al. 2013, Cosmol. Astropart., 7, 008
Hernández-Monteagudo, C., Ma, Y.-Z., Kitaura, F. S., et al. 2015, Phys. Rev. Lett., 115, 191301
Hill, J. C., & Sherwin, B. D. 2013, Phys. Rev. D, 87, 023527
Ho, S., Dedeo, S., & Spergel, D. 2009, ArXiv e-prints [arXiv:0903.2845]
Hurier, G., Macías-Pérez, J. F., & Hildebrandt, S. 2013, A&A, 558, A118

Kitaura, F.-S., Angulo, R. E., Hoffman, Y., & Gottlöber, S. 2012, MNRAS, 425, 2422
Komatsu, E., & Kitayama, T. 1999, ApJ, 526, L1
Komatsu, E., & Seljak, U. 2001, MNRAS, 327, 1353
Komatsu, E., & Seljak, U. 2002, MNRAS, 336, 1256
Lacasa, F. 2014, ArXiv e-prints [arXiv:1406.0441]
Mantz, A. B., von der Linden, A., Allen, S. W., et al. 2015, MNRAS, 446, 2205
Mather, J. C., Fixsen, D. J., Shafer, R. A., Mosier, C., & Wilkinson, D. T. 1999, ApJ, 512, 511
Mo, H. J., & White, S. D. M. 1996, MNRAS, 282, 347
Nagai, D., Kravtsov, A. V., & Vikhlinin, A. 2007, ApJ, 668, 1
Navarro, J. F., Frenk, C. S., & White, S. D. M. 1997, ApJ, 490, 493
Ostriker, J. P., & Vishniac, E. T. 1986, ApJ, 306, L51
Peebles, P. J. E. 1980, The large-scale structure of the universe (Princeton, N.J.: Princeton University Press)
Planck Collaboration XI. 2011, A&A, 536, A11
Planck Collaboration XV. 2014, A&A, 571, A15
Planck Collaboration XXI. 2014, A&A, 571, A21
Planck Collaboration XXIX. 2014, A&A, 571, A29
Planck Collaboration I. 2016, A&A, 594, A1
Planck Collaboration IX. 2016, A&A, 594, A9
Planck Collaboration XIII. 2016, A&A, 594, A13
Planck Collaboration XXII. 2016, A&A, 594, A22
Planck Collaboration XXIII. 2016, A&A, 594, A23
Planck Collaboration XXIV. 2016, A&A, 594, A24
Planck Collaboration XXVII. 2016, A&A, 594, A27
Remazeilles, M., Delabrouille, J., & Cardoso, J.-F. 2011, MNRAS, 410, 2481
Sayers, J., Mroczkowski, T., Zemcov, M., et al. 2013, ApJ, 778, 52
Shaw, L. D., Rudd, D. H., & Nagai, D. 2012, ApJ, 756, 15
Sievers, J. L., Hlozek, R. A., Nolta, M. R., et al. 2013, Cosmol. Astropart., 10, 060
Soergel, B., Flender, S., Story, K. T., et al. 2016, MNRAS, 461, 3172
Sugiyama, N. S., Okumura, T., & Spergel, D. N. 2017, Cosmol. Astropart., 1, 057
Sunyaev, R. A., & Zeldovich, Y. B. 1972, Comm. Astrophys. Space Phys., 4, 173
Taburet, N., Hernández-Monteagudo, C., Aghanim, N., Douspis, M., & Sunyaev, R. A. 2011, MNRAS, 418, 2207
Tinker, J., Kravtsov, A. V., Klypin, A., et al. 2008, ApJ, 688, 709
Wilson, M. J., Sherwin, B. D., Hill, J. C., et al. 2012, Phys. Rev. D, 86, 122005